IMPACT OF A PURINA FRACTAL ARRAY GEOMETRY ON BEAMFORMING PERFORMANCE AND COMPLEXITY

P. Karagiannakis[1], S. Weiss[1], G. Punzo[2], M. Macdonald[2], J. Bowman[3], and R.W. Stewart[1]

[1]Department of Electronics & Electrical Engineering
[2]Advanced Space Concepts Laboratory
University of Strathclyde, Glasgow G1 1XW, Scotland
[3]Steepest Ascent Ltd., 94 Duke Street, Glasgow G4 0UW, Scotland
{philipp.karagiannakis,s.weiss,giuliano.punzo,malcolm.macdonald.102,r.stewart}@strath.ac.uk

ABSTRACT

This paper investigates the possible benefits of using a Purina fractal array for beamforming, since this particular fractal has recently been suggested as the flight formation for a fractionated space craft. We analyse the beam pattern created by this, and define power concentration as measure of focussing the main beam of a multi-dimensional array. Using this performance metric and the computation cost of the array, a comparison to full lattice arrays is made. We quantify the significant benefits of the Purina array offered over a full lattice array of same complexity particularly at lower frequencies, and the complexity advantages over full lattice arrays of same aperture, particularly if energy is to be concentrated within a small angular spread.

***Index Terms*—** Fractal arrays; beamforming; computational complexity; performance metrics.

1. INTRODUCTION

Recent developments in nano-satellites have sparked a resurgence in the popularity of formation flying and fractionated spacecraft, where the functionality of a standard satellite is replaced by a swarm of smaller devices. The ability to fly such spacecraft reliably in complex formations [1] has triggered interest in utilising fractal geometries [2, 3], which can also be utilised as antenna arrays [4, 5].

The computational cost of processing data rises quickly with an array's dimension, particularly if it involves broadband processing with complex algorithms [6]. Therefore, various efforts have been undertaken to reduce this cost, which includes low-cost versions of more complex algorithms such as e.g. effort to reduce recursive least-squares methods to stable algorithms of linear order [7]. Also, thinning of arrays, whereby some spatial elements are discarded from processing,have proven advantageous [8, 9]. Another approach is to construct a sparse, non-uniform array form the outset.
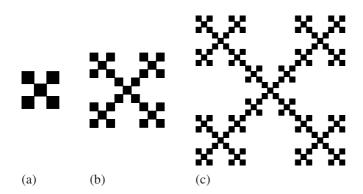
Efforts spanning half a century have investigated the notion of non-uniform sparse arrays [10, 11]. Methods covered in previous works include logarithmically spacing array elements [12], octave-scaling [13, 14] of the array aperture and building up antenna arrays from randomly spaced elements [15]. In [5] fractal antenna arrays have been shown to combine the attractive features of both periodic and random arrays, which provides a systematic and practical approach to the design of deterministic fractal antennas.

The benefits of fractal geometries as demonstrated by [5] have been exploited in [3] for satellite formation flying based on fractal geometries. Therefore, this paper analyses the impact of the fractal geometry of such an array when utilised for beamforming, with a comparison to equivalent full, i.e. non-sparse, lattice arrays of equivalent complexity or aperture. The beam pattern generally offers a good visualisation of the directivity of an array, but makes comparisons for 2D or 3D arrays difficult due to their dependency on azimuth, elevation and frequency. To reduce this parameter space, in this paper we introduce a metric termed power concentration, which assesses the power dissipated within a cone aligned with the array's look direction, i.e. an assessment how much of the radiated power will reach a specific foot print defined by a — likely small — angular spread. Using this metric the performance for beamformers of varying complexity can be compared, independent of the number of sensor elements used to form the array and across a range of frequencies.

Below, Sec. 2 provides a brief review of the construction of a Purina array and a coarse comparison to full lattice arrays. The beam pattern of an array is discussed in Sec. 3, which lays the basis for defining the power concentration metric in Sec. 4 and its application the Purina array in Sec. 5.

2. FRACTAL ARRAY

Fractals and fractal geometry [16] were introduced to describe naturally occurring irregular but self-similar structures, and have found bearing in a wide range of scientific and engineering fields since. For the particular application of fractionated space craft [2, 3], the Purina fractal has been found to be ad-

(a)   (b)   (c)

Fig. 1. First three stages of growth of the Purina fractal array for (a) $P = 1$, (b) $P = 2$, and (c) $P = 3$.

vantageous due to its rapid growth coupled with a relatively low number of elements.

Deterministic fractal geometries are constructed from a generating sub-array at growth scale, $P = 1$, with higher growth scales derived by repetitions [5]. For the Purina fractal the generating sub-array at growth scale $P = 1$ is a 3×3 matrix S_1,

$$\mathrm{S}_1 = \begin{bmatrix} 1 & 0 & 1 \\ 0 & 1 & 0 \\ 1 & 0 & 1 \end{bmatrix} \quad . \tag{1}$$

where a unit entry means that an array element is present, while a zero indicates the absence of an element. The array fractal pattern S_P at an arbitrary growth scale $P \in \mathbb{N}, P \geq 2$ is given by

$$\mathrm{S}_P = \mathrm{S}_1 \otimes \mathrm{S}_{P-1} \quad , \tag{2}$$

with $\otimes$ denoting the Kronecker product. The first three stages of growth of the Purina fractal are shown in Fig. 1.

Some of the array parameters such as element numbers and aperture can be derived from the fractal's repetition in (2). Assume that the generating sub-array contains N_1 elements and that the minimum element distance is d. Note that according to (1) and Fig. 1, this minimum distance is achieved by diagonally positioned neighbours. Therefore at growth scale P, the N_P elements will form a square $D_P \times D_P$ aperture with

$$N_p = N_1^P \quad , \qquad D_P = \tilde{D}_1^P \left(\frac{d}{\sqrt{2}} \right) \quad , \tag{3}$$

whereby for the Purina sub-array in (1), $N_1 = 5$ and dimension $\tilde{D}_1 = 3$. The parameters in (3) will directly impact on the complexity and spatial resolution of the fractal array.

To compare complexity and aperture to a full $N \times N$ lattice array, we first consider the reduction in complexity if aiming for the same aperture D_p as a Purina array at scale P. This requires $N = \frac{D_P}{d}$, yielding a relative complexity

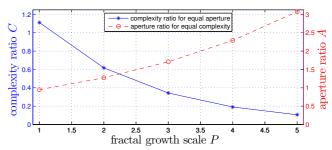$$C = \frac{N_P}{N^2} = \frac{N_1^P}{D_1^{2P}} = \frac{2 N_1^P}{\tilde{D}_1^{2P}} = 2 \left(\frac{5}{9} \right)^P \tag{4}$$

Fig. 2. Comparison between Purina fractal array for growth scales $P = 1 \ldots 5$ and equivalent full scale lattice arrays.

	fractal	full lattice array	
	$P = 3$	11×11	19×19
number of elements	125	121	361
aperture / d	19.07	11.00	19.00

Table 1. Comparison of complexity and aperture of Purina fractal ($P = 3$) with equivalent full lattice arrays.

for the Purina fractal under the assumption of linear processing. If adaptive processing with e.g. recursive least squares-type algorithms of quadratic order in the coefficients is performed, the advantage would be further biased towards the Purina array.

Secondly, given a Purina fractal at grow scale P with aperture D_P, a full lattice array to equal its complexity N_p would occupy a $\sqrt{N_P}d \times \sqrt{N_P}d$ aperture. Therefore

$$A = \frac{D_P}{\sqrt{N_P}d} = \frac{1}{\sqrt{2}} \left(\frac{\tilde{D}_1}{\sqrt{N_1}} \right)^P = \frac{1}{\sqrt{2}} \left(\frac{3}{\sqrt{5}} \right)^P \tag{5}$$

represents the increase in aperture afforded by the Purina fractal compared to a full lattice array of equal complexity. This ratio, together with decrease in complexity, is demonstrated in Fig. 2. The equivalent full lattice arrays for a Purina fractal at growth scale $P = 3$ are listed in Tab. 1.

The comparison based on (4) and (5) suggest clear advantages for the Purina array, but omits effects such as the effects of grating lobes to the fractal array's sparse element population. Therefore, below metrics for the assessment of such arrays will be discussed, with the beam patterns to be defined in Sec. 3 leading to a new proposed metric in Sec. 4.

3. ARRAY ANALYSIS AND GAIN RESPONSE

In order to analyse general arrays, and particularly the Purina array discussed in Sec. 2, we below determine the gain response or beam pattern of the array w.r.t. frequency and angle of arrival. Sec. 3.1 first reviews the spatial and temporal sampling of a narrowband signal, before steering vectors are defined in Sec. 3.2. This leads to the formulation of the general beam pattern in Sec. 3.3 with an example for the Purina array.

2

The analysis below is performed for an array acting as a receiver, motivated by traditional notation of sources and corresponding steering vectors. The design of a beamformer for transmission, which is the aim of this paper, is analogous, and we will return to this in Sec. 4.

3.1. Spatial and Temporal Sampling

To spatially sample a far-field signal $x(t)$ with power spectral density $S_{xx}(j\omega) = 0 \quad \forall |\omega| \geq \omega_{\max}$ by an array with M elements defined by element positions $\mathbf{r}_m$, $m = 1 \ldots M$, at least two array elements have to fulfill the minimum requirement

$$\min_{m,\mu} \|\mathbf{r}_m - \mathbf{r}_\mu\|_2 \leq \frac{\lambda_{\min}}{2} \tag{6}$$

in order to obtain an unambiguous representation free of spatial aliasing. The minimum wavelength

$$\lambda_{\min} = \frac{2\pi c}{\omega_{\max}} \tag{7}$$

relates to the maximum angular frequency $\omega_{\max}$ via the propagation speed c in the medium.

If the array acquires the continuous time signal $x(t)$, it will, due to its emanating from the far-field, arrive at the array in a planar wavefront characterised by a normal vector $\mathbf{k}$,

$$\mathbf{k} = \begin{bmatrix} \sin\vartheta\cos\varphi \\ \sin\vartheta\sin\varphi \\ \cos\vartheta \end{bmatrix} \quad , \tag{8}$$

with azimuth φ and elevation ϑ as defined in Fig. 3. Therefore the delay experienced by the mth array element relative to the origin is

$$x_m(t) = x(t - \Delta T_m) = x(t - \frac{\mathbf{k}^{\mathrm{T}}\mathbf{r}_m}{c}) \quad , \tag{9}$$

where $\mathbf{k}/c$ is also known as the slowness vector.

Temporal sampling of $x_m(t)$ with a sampling period T_{s} leads to

$$\begin{aligned} x_m[n] &= x_m(nT_{\mathrm{s}} - \Delta T_m) = x_m((n - \frac{\mathbf{k}^{\mathrm{T}}\mathbf{r}_m}{cT_{\mathrm{s}}})T_{\mathrm{s}}) \\ &= x_m[n - \tau_m] \end{aligned} \tag{10}$$

where $\tau_m = \frac{\mathbf{k}^{\mathrm{T}}\mathbf{r}_m}{cT_{\mathrm{s}}}$. Specifically considering a complex exponential $x(t) = e^{j\omega t}$,

$$x_m[n] = e^{j\omega(n - \tau_m)T_{\mathrm{s}}} = e^{j\Omega n}e^{-j\Omega\tau_m} \quad , \tag{11}$$

for this narrowband excitation the time delay ΔT_m turns into a phase shift $\Omega\tau_m$.
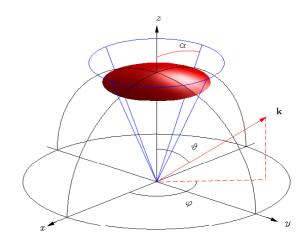

Fig. 3. Coordinate system with a planar array located at the origin in the xy plane; the cone serves to measure the dissipated power within an elevation angle α by integrating over the shaded surface.

3.2. Steering Vector and Quiescent Beamformer

For the narrowband excitation in (11), concatenating all sensor signals $x_m[n]$ into a vector $\mathbf{x}[n]$,

$$\mathbf{x}[n] = \begin{bmatrix} x_1[n] \\ x_2[n] \\ \vdots \\ x_M[n] \end{bmatrix} = e^{j\Omega n}\begin{bmatrix} e^{-j\Omega\tau_1} \\ e^{-j\Omega\tau_2} \\ \vdots \\ e^{-j\Omega\tau_M} \end{bmatrix} = \sqrt{M}e^{j\Omega n}\mathbf{s}_{\varphi,\vartheta,\Omega} \tag{12}$$

yields the unit norm steering vector $\mathbf{s}_{\varphi,\vartheta,\Omega}$, which uniquely characterises a source of normalised angular frequency Ω coming from a direction defined by azimuth φ and elevation ϑ through the dependency on $\mathbf{k}$.

To calculate beamforming coefficients $\mathbf{w}$ that fulfill the contraint $\mathbf{w}^{\mathrm{T}}\mathbf{s}_{\Omega_0,\varphi_0,\vartheta_0} = 1$ while minimising the impact of isotropic noise, the quiescent solution is the matched filter, $\mathbf{w} = \mathbf{s}_{\Omega_0,\varphi_0,\vartheta_0}$.

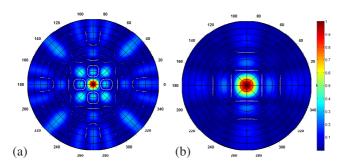### 3.3. Beam Pattern

To characterise a beamformer with coefficient vector $\mathbf{w}$ adjusted for a source with parameter set $\{\Omega_0, \varphi_0, \vartheta_0\}$, the beam or directivity pattern

$$G(\Omega, \varphi, \vartheta) = \mathbf{w}^{\mathrm{T}}\mathbf{s}_{\Omega,\varphi,\vartheta} \tag{13}$$

measures the gain with respected to potential sources over a grid of frequencies and angles of arrival by scanning the coefficient vector with the resulting set of steering vectors.

For the Purina array, assuming critical sampling in space, such that (6) holds with equality, and in time with $f_{\mathrm{s}} = 2f_{\max}$, Fig. 4(a) show the resulting beam pattern at growth scale $P = 3$ for a beamformer looking towards broadside at

Fig. 4. Beam patterns for (a) Purina fractal at growth scale $P = 3$ and (b) 11×11 full lattice array of similar complexity.

Fig. 5. Power concentration curves for the Purina fractal array with $P = 3$, compared to a number of equivalent full lattice arrays of same complexity (11×11) and aperture (19×19) at normalised angular frequencies (a) $\Omega = \frac{\pi}{2}$ and (b) $\Omega = \frac{\pi}{8}$.

$\Omega = \frac{\pi}{2}$. With 125 elements, this array has a similar complexity but a larger aperture than the 11×11 full lattice array in Fig. 4(b) with its 121 elements. As a result of this increased aperture, the fractal array's main beam appears more focused than the full square lattice array, offering a better resolution. However, Fig. 4 also highlights the grating lobes which appear in the Purina array's beam pattern due to partial spatial undersampling, an effect that is absent from the full lattice structure in Fig. 4(b).

4. POWER CONCENTRATION

While the beam pattern is very descriptive, its dependency on azimuth φ, elevation ϑ and normalised angular frequency Ω makes a comparison between different arrays difficult. Since the purpose of the array created by a fractionalised space craft is to concentrate as much of the transmitted power onto a limited footprint at the receiver, we below introduce a metric that captures the power which an array can dissipate within a cone of opening angle α, for simplicity towards broadside as look-direction, as shown in Fig. 3.
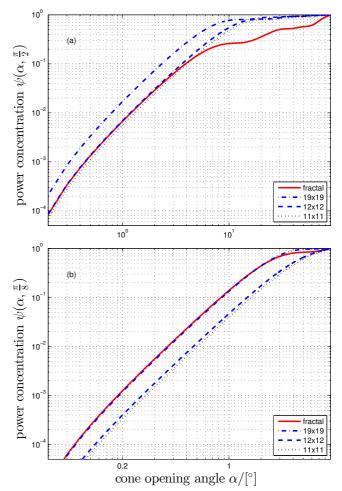
The transmitted power within a cone of opening angle α is obtained by integrating the square beam pattern over the shaded area in Fig. 3, which is formed by a hemisphere in the far-field of the array intersecting the cone, such that

$$\psi(\alpha, \Omega) = \int\limits_{0}^{2\pi} \int\limits_{0}^{\alpha} |G(\vartheta, \varphi, \Omega)|^2 \sin\vartheta \; \partial\vartheta \; \partial\varphi \quad . \tag{14}$$

Normalising this power by the total transmit power dissipated across the hemisphere at a specific frequency Ω, $\psi(\frac{\pi}{2}, \Omega)$,

$$\rho(\alpha, \Omega) = \frac{\psi(\alpha, \Omega)}{\psi(\frac{\pi}{2}, \Omega)} \tag{15}$$

forms a measure $\rho(\alpha, \Omega)$, that is monotonically increasing with $\rho(0, \Omega) = 0$ and $\rho(\frac{\pi}{2}, \Omega) = 1$ akin to a cummulative density function. We hereby refer to this measure as power concentration, and the ability of an array, at a frequency Ω, to better direct energy closer to the main beam will result in a faster rising power concentration $\rho_1(\alpha, \Omega)$ that majorises the power concentration $\rho_2(\alpha, \Omega) \leq \rho_1(\alpha, \Omega)$, $\forall \alpha, \Omega$ of a less directive array.

5. SIMULATIONS AND RESULTS

The power concentration metric defined in Sec. 4 is used to compare a Purina fractal array at growth scale $P = 3$ with full lattice arrays of equivalent complexity and performance, as characterised in Tab. 1. Fig. 5 shows the power concentration curves at $\Omega = \frac{\pi}{2}$ and $\Omega = \frac{\pi}{8}$. In general, with increasing array size, power concentration curves are majorised except for the fractal array, where grating lobes particularly at higher frequencies, such as $\Omega = \frac{\pi}{2}$ disturb convergence for increasing cone angles α. However, for $\Omega = \frac{\pi}{2}$ in Fig. 5(a), at low angles α — relating to a sensibly sized footprint when emitting from an orbiting fractionated space craft to ground — the power concentration of the Purina array outperforms the
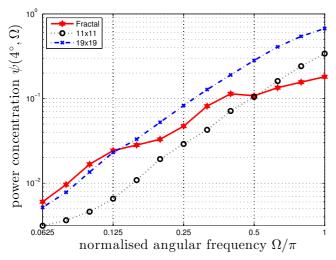
4

Fig. 6. Power concentration for fixed cone opening $\alpha = 4°$ and variable normalised angular frequency Ω.

11×11 array of equal complexity and performs close to a 12×12 full lattice array.

At a normalised angular frequency $\Omega = \frac{\pi}{8}$ — a fraction of $\frac{1}{16}$ of the sampling rate —, the aperture of the array becomes the dominating factor in determining spatial resolution. As evident from Fig. 5(b), the Purina array performes comparable to the 19×19 full lattice array of equal aperture, while significantly outperforming the 11×11 system.

To demonstrate power concentration over the entire frequency range, we measure the power concentrated within the footprint of a cone with opening angle $\alpha = 4°$. The result for variable Ω is shown in Fig. 6 whereby for the majority of frequencies the Purina fractal array is able to concentrate a higher proportion of its energy than a full lattice array of similar complexity. Compared to a full lattice array of equivalent spatial aperture, containing almost 3-times as many elements, the fractal array offers comparable performance in the lower frequency ranges.

6. CONCLUSION

The Purina fractal array, based on its use as formation for a fractionated spacecraft, has been utilised in this paper as a beamformer, which we have compared in terms of complexity and aperture to full lattice array beamformers with comparable system parameters. To better assess the array's ability to concentrate transmit power within a cone, power concentration has been introduced as a metric, which can be derived from the array's beam pattern. The dependency on azimuth and elevation is thereby compressed into a single variable. The analysis performed with this metric indicates that, compared to full lattice arrays, the fractal geometry has very distinct advantages if energy has to be concentrated within a small angular spread, particularly at lower frequencies.

7. REFERENCES

[1] M.A. Peck, B. Streetman, C.M. Saaj, and V. Lappas, "Spacececraft formation flying using Lorentz forces", *J. British Interplanetary Society*, **60**:263–267, 2007.

[2] G. Punzo, D.J. Bennett, and M. Macdonald, "A fractally fractionated spacecraft,", in *62nd Int. Astronautical Congress*, Cape Town, South Africa, Oct. 2011.

[3] G. Punzo, P. Karagiannakis, M. Macdonald, D. Bennet, and S. Weiss, "Enabling and exploiting self-similar central symmetry formations," *submitted to IEEE Trans. Aerospace & Electronic Systems*, 2012.

[4] C. Puente-Baliarda and R. Pous, "Fractal design of multiband and low side-lobe arrays", *IEEE Trans. Antennas & Propagation*, **44**(5):730–739, May 1996.

[5] D. H. Werner and R. Mittra, "The theory and design of fractal antenna arrays," in *Frontiers in Electromagnetics*, pp. 94–203, Wiley-IEEE Press, 2000.

[6] W. Liu and S. Weiss, *Wideband Beamforming — Concepts and Techniques*, Wiley, 2010.

[7] I. Skidmore and I.K. Proudler, "The KaGE RLS algorithm," *IEEE Trans. Signal Processing*, **51**(12):3094-3104, Dec. 2003.

[8] R.M. Leahy and B.D. Jeffs, "On the design of maximally sparse beamforming arrays," *IEEE Trans. Antennas and Propagation*, **39**(8):1178–1187, Aug. 1991.

[9] G. Cardone, G. Cincotti, and M. Pappalardo, "Design of wide-band arrays for low side-lobe level beam patterns by simulated annealing," *IEEE Trans. Ultrasonics, Ferroel. & Freq. Cont.*, **49**(8):1050–1059, Aug. 2011.

[10] D. King, R. Packard, and R. Thomas, "Unequally-spaced, broad-band antenna arrays," *IRE Trans. Antennas & Propagation*, **8**(4):380–384, July 1960.

[11] A.L. Maffett, "Array factors with nonuniform spacing parameter," *IRE Trans. Antennas & Propagation*, **10**(2):131–136, Mar. 1962.

[12] M. Van der Wal and D. de Vries, "Design of logarithmically spaced constant-directivity transducer arrays," *IEEE Trans. Ultrasonics, Ferroel. & Freq. Cont.*, **44**(6):497–507, June 1996.

[13] S. Weiss, R.W. Stewart, and Wei Liu, "A broadband adaptive beamformer in subbands with scaled aperture," in *36th Asilomar SSC Conf.*, **2**:1298–1302, Nov. 2002.

[14] H. L. Van Trees, *Optimum Array Processing*, Wiley, New York, 2004.

[15] Y.T. Lo, "A mathematical theory of antenna arrays with randomly spaced elements," *IEEE Trans. Antennas & Propagation*, **12**(3):257–268, May 1964.

[16] B.B. Mandelbrot, *The Fractal Geometry of Nature*, Henry Holt and Company, 1983.

[17] J. Leitner, "Formation flying: The future of remote sensing from space", NASA Tech. Report, Goddard Space Flight Center, MD, 2004.